

RESEARCH ARTICLE

10.1002/2014JD022316

Key Points:

- Great Lakes and surrounding land contribute up to one third of local rainfall
- RegCM does not capture observed evapotranspiration feedbacks
- Warm LST biases enhance convective precipitation by 2.5% per degree K

Correspondence to:

A. M. Bryan,
ambrya@umich.edu

Citation:

Bryan, A. M., A. L. Steiner, and D. J. Posselt (2015), Regional modeling of surface-atmosphere interactions and their impact on Great Lakes hydroclimate, *J. Geophys. Res. Atmos.*, 120, 1044–1064, doi:10.1002/2014JD022316.

Received 14 JUL 2014

Accepted 30 DEC 2014

Accepted article online 7 JAN 2015

Published online 12 FEB 2015

Regional modeling of surface-atmosphere interactions and their impact on Great Lakes hydroclimate

A. M. Bryan¹, A. L. Steiner¹, and D. J. Posselt¹¹Department of Atmospheric, Oceanic, and Space Sciences, University of Michigan, Ann Arbor, Michigan, USA

Abstract Land and water surfaces play a critical role in hydroclimate by supplying moisture to the atmosphere, yet the ability of climate models to capture their feedbacks with the atmosphere relative to large-scale transport is uncertain. To assess these land-lake-atmosphere feedbacks, we compare the controls on atmospheric moisture simulated by a regional climate model (RegCM) with observations and reanalysis products for the Great Lakes region. Three 23 year simulations, driven by one reanalysis product and two general circulation models, are performed. RegCM simulates wetter winters and drier summers than observed by up to 31 and 21%, respectively. Moisture advection exhibits similar biases, suggesting the contribution of external sources. Land surface fluxes account for nearly one third of summer precipitation according to two reanalysis products. RegCM underestimates reanalysis evapotranspiration by nearly 50%; however, the reanalyses overestimate measurements at three FLUXNET sites by up to a factor of 2, which may explain the model-reanalysis differences. Neither RegCM nor the reanalyses capture the spatial variability in land evapotranspiration observed across the three FLUXNET sites, indicating a source of model uncertainty. In addition, RegCM underestimates the observed evapotranspiration response to its atmospheric drivers such as vapor pressure deficit and temperature. Over the lakes, one model member overestimates convective precipitation caused by enhanced evaporation under warm lake surface temperatures, highlighting the need for accurate representation of lake temperature in the surface boundary condition. We conclude that climate models, including those driving reanalyses, underestimate the observed surface-atmosphere feedbacks and their influence on regional hydroclimate.

1. Introduction

The Laurentian Great Lakes collectively represent the largest continental water bodies in the world and thus have a profound influence on the local and regional hydroclimate [Changnon and Jones, 1972; Bates et al., 1993; Scott and Huff, 1996; Li et al., 2010; Notaro et al., 2013a]. One classic example of local phenomenon is lake-effect snow, when warm lake surface temperatures beneath the cold winter air enhance evaporation from the lakes and precipitation just beyond the shoreline [Scott and Huff, 1996; Wright et al., 2013]. On a regional scale, the lakes can perturb atmospheric circulation patterns and other mesoscale features [Pettersen and Calabrese, 1959; Sousounis and Fritsch, 1994; Notaro et al., 2013a]. In addition to water bodies, the land surface exerts a substantial influence on regional climate, especially over dense terrestrial vegetation [Bonan, 2008]. While the impacts of the land and lakes on regional weather and climate have been well documented, few studies have assessed and distinguished the relative impacts of the Great Lakes and the surrounding land on the regional hydroclimatology. In fact, it has long been assumed that precipitation derives primarily from moisture transported in from long distances relative to local evapotranspiration [Budyko, 1974; Trenberth, 1999; Li et al., 2010]. While this assumption may be true in most regions dominated by land, the Great Lakes region may stand as an exception due to the vastness of its water bodies. This study aims to quantify the impacts of the land and lake surfaces on Great Lakes hydroclimate and evaluate the ability of a regional climate model to capture these feedbacks and their drivers.

Land and lake surfaces interact with the atmosphere in distinct ways to modify local hydroclimate. Moisture precipitated onto land surfaces can either recycle back to the atmosphere via evaporation [Brubaker et al., 1993] or run off into the lakes. Land surface moisture evaporates readily with increased solar energy input and atmospheric warming; thus, evaporation rates peak in the midsummer following the seasonal cycle of solar insolation. Water bodies respond slowly to solar insolation and atmospheric conditions, and lake evaporation peaks in the late fall as the air cools [Changnon and Jones, 1972; Derecki, 1981; Lofgren, 1997].

The influence of the land surface on atmospheric conditions depends on the coupling strength between the land and atmosphere. Land-atmosphere coupling, where small perturbations in the land surface feed back to the atmosphere, has been defined as energy limited or soil moisture limited [Seneviratne *et al.*, 2010; Mei and Wang, 2012]. Energy-limited regimes are limited by the surface energy balance, temperatures, and incoming radiation versus the amount of water availability. The northern location of the Great Lakes region (above 40°N) suggests that evapotranspiration is typically energy limited [Tawfik and Steiner, 2013], and generally, these regions tend to have weak land-atmosphere coupling relative to soil moisture-limited regions.

Several studies have applied regional climate models (RCMs) to the Great Lakes region to assess the complex lake-atmosphere interactions [Bates *et al.*, 1993, 1995; Goyette *et al.*, 2000; Lofgren, 2004; Zhong *et al.*, 2012; Notaro *et al.*, 2013a, 2013b]. Zhong *et al.* [2012] used the Penn State-National Center for Atmospheric Research (NCAR) Mesoscale Model version 5, driven by multiple boundary conditions, and found that the model accurately represents moisture fluxes estimated by North American Regional Reanalysis (NARR). Notaro *et al.* [2013b] found that the Abdus Salam International Centre for Theoretical Physics regional climate model (RegCM) reproduces lake-effect snowfall and ice coverage over the Great Lakes in the winter when using an interactive lake module. When coupled with the NCAR Community Land Model (CLM), RegCM identifies relatively weak coupling over the Great Lakes and elsewhere in the U.S. [Mei *et al.*, 2013]. However, while RCMs generally reproduce atmospheric conditions, their ability to accurately simulate land-lake-atmosphere feedbacks remains uncertain [Jimenez *et al.*, 2014].

In this study, we use RegCM coupled with CLM to investigate the land- and lake-atmosphere feedbacks on hydroclimate in the Great Lakes region. We first evaluate the simulated moisture budget components (precipitation, evaporation, and moisture transport) against a suite of observational and reanalysis data sets to provide a baseline understanding of the model performance (section 3). This evaluation also compares moisture fluxes from the land and lake surfaces and surrounding regions to identify the relative sources and sinks of atmospheric moisture in the region. We then quantify and evaluate land-lake-atmosphere feedbacks by estimating local moisture recycling and by comparing observed and simulated relationships between land and lake moisture fluxes and their drivers (section 4). This manuscript expands upon previous work [e.g., Zangvil *et al.*, 2004; Li *et al.*, 2010; Zhong *et al.*, 2012; Notaro *et al.*, 2013a] by comparing the land and lakes as atmospheric moisture sources and identifying the sources of error in the simulated moisture budget. The overall goal of this manuscript is to improve our understanding of the controls on atmospheric moisture in the Great Lakes region, particularly the role of the land and lake surfaces.

2. Methods

2.1. Model and Simulation Design

We simulate atmospheric and surface conditions, processes, and interactions using RegCM version 4.3.4 [Giorgi *et al.*, 2012] coupled with CLM version 3.5 [Oleson *et al.*, 2004]. Precipitation is simulated with both large-scale and convective precipitation parameterizations. Large-scale (i.e., nonconvective) precipitation is generated by the Subgrid Explicit Moisture Scheme [Pal *et al.*, 2000], which simulates precipitation instantaneously where and when relative humidity supports cloud formation and cloud water content exceeds an empirically derived temperature-dependent threshold. Convective precipitation follows the Grell [1993] scheme with the closure assumption of Fritsch and Chappell [1980].

The CLM land surface model represents vegetation with four to six plant functional types (PFTs) per model grid cell. Land cover types and PFTs are distinguished by several attributes affecting land-atmosphere interactions, including optical properties (e.g., albedo), aerodynamic roughness, and several factors that influence soil moisture exchange. While CLM contains a lake model [Zeng *et al.*, 2002] that computes prognostic lake surface temperatures (LSTs) and ice coverage, this model was not implemented over the Great Lakes due to the land/ocean mask, which sets the Great Lakes to ocean values. As a result, LSTs are provided by the driving GCM. If this is not provided for a specific boundary condition, then RegCM estimates LSTs by interpolating ocean sea surface temperatures (SSTs) from the nearest coastlines. Only one of the three boundary conditions used in the present study utilizes this interpolation method. The lack of a coupled lake model limits the ability of the model to simulate future atmospheric conditions, as lake-atmosphere feedbacks are not included. The implications of this interpolation on lake-atmosphere feedbacks are discussed in sections 3.2 and 4.3.

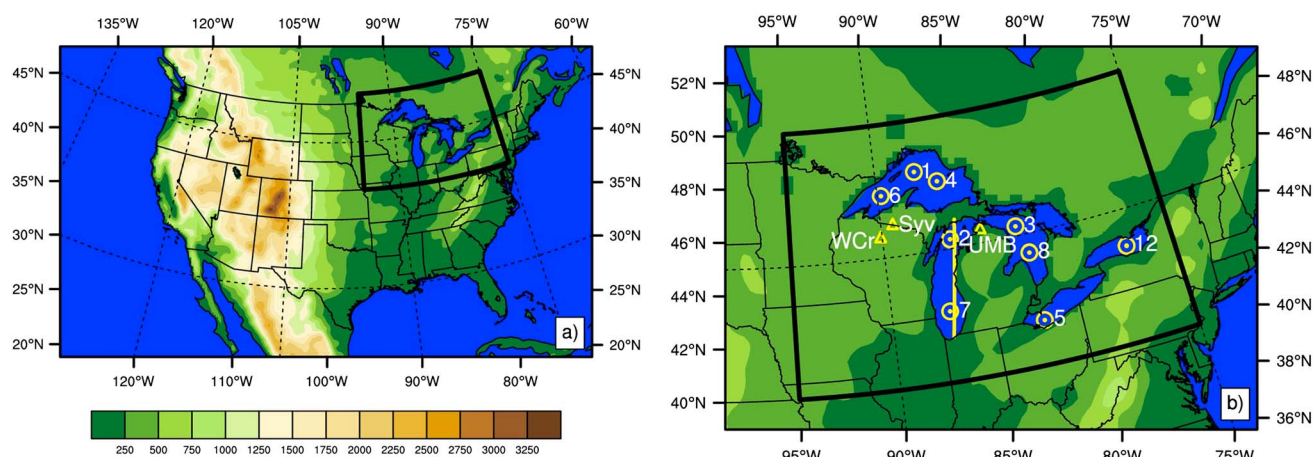


Figure 1. (a) Simulation domain and (b) Great Lakes Watershed (GLW) analysis domain (40–50°N, 95–75°W, black outline) with FLUXNET tower (triangles) and National Data Buoy Center (NDBC) buoy (dotted circles) locations. Colored contours represent elevation in meters. UMB, WCr, and Syv denote the University of Michigan Biological Station, Willow Creek, and Sylvania Wilderness Area FLUXNET sites, respectively. The numbered buoy identifiers correspond to the last 1–2 digits of the station ID listed in Table 1. The yellow line spanning lengthwise through Lake Michigan denotes the latitudinal band used in the cross sections in Figure 13.

We simulate climate and surface interactions in the continental United States (Figure 1a) for the 23 year historical period ranging from January 1980 to December 2002. Simulating the full continental U.S. allows the model to capture synoptic-scale weather patterns and topography, but we constrain our analysis to the subregion encompassing the Great Lakes Watershed (40–50°N, 95–75°W; Figure 1b), hereafter referred to as the GLW domain to distinguish from the full simulation domain. Model simulations are at 25 km horizontal grid spacing and contain 18 sigma levels up to 50 hPa. In addition to the 23 year analysis period, we initialized the model with a 12 and 20 month spin-up with the length of spin-up depending on availability of input data.

We conduct three simulations constrained by different lateral boundary conditions and SST data sets to assess the impact of input selection on simulation results and identify the effect of synoptic weather patterns on moisture transport (section 3.3). First, we drive RegCM with the European Centre for Medium-Range Weather Forecasts (ECMWF) Reanalysis (ERA) Interim reanalysis data set (hereafter RCM-ERA) [Dee et al., 2011] to accurately capture large-scale conditions. In addition to ERA reanalysis, we drive the model with two general circulation models (GCMs): the National Oceanic and Atmospheric Administration (NOAA) Geophysical Fluid Dynamics Laboratory Earth System Model using the Modular Ocean Model version 4.1 (GFDL-ESM2M) (RCM-GFDL) [Dunne et al., 2012, 2013] and the Met Office Hadley Centre Hadley Global Environment Model 2 Earth System model (HadGEM2-ES) (RCM-HADGEM) [Collins et al., 2011; Martin et al., 2011]. RCM-ERA derives SSTs from the NOAA National Centers for Environmental Prediction (NCEP) 2-D-Var (through June 2001) and the NOAA optimum interpolation sea surface temperature (OISST, version 2; since July 2001) data sets [Dee et al., 2011]. Simulated skin temperatures are used for ocean, land, and lake surface temperatures in RCM-GFDL. While simulated SSTs from the parent model are used for the RCM-HADGEM simulation, we note that the data set excludes lake surface temperatures, and thus, RegCM interpolates between the ocean coastlines.

2.2. Ancillary Data Sets

Observational data sets used in this study derive from four sources: (1) gridded observation products, (2) flux towers, (3) lake buoys, and (4) satellites. We evaluate RegCM temperature and precipitation output with station data gridded globally at 0.5° resolution by the Climatic Research Unit of the University of East Anglia (CRU) [New et al., 2000] and from the University of Delaware (UDel) [Willmott and Matsuura, 2001]. While the gridded station data products do not have robust measurements over the lakes [Holman et al., 2012], the lakes make up only 11.8% of the analysis domain and so any biases caused by missing data are relatively small (< 5%). In addition, station gauges tend to underestimate snowfall due to wind undercatch [Legates and Willmott, 1990], which is accounted for in the UDel data set.

Table 1. Location, Data Availability, and Measurement Information for the Point-Based Observational Data Sets Used in This Study^a

	Location	Years Available	T_{air} Height	$T_{\text{soil}}/T_{\text{lake}}$ Depth
<i>Towers</i>				
UMB	45.56N, 84.71W	1999 to the present	46 m	2 cm
WCr	45.81N, 90.08W	1999 to the present	30 m	0 cm
Syv	46.24N, 89.35W	2001 to 2008	36 m	5 cm
<i>Buoys</i>				
45001 (Superior)	48.06N, 87.78W	1980 to the present	4.0 m	0.6 m
45002 (Michigan)	45.34N, 86.41W	1980 to the present	4.0 m	1.0 m
45003 (Huron)	45.35N, 82.84W	1980 to the present	3.2 m	1.0 m
45004 (Superior)	47.58N, 86.69W	1980 to the present	4.0 m	1.0 m
45005 (Erie)	41.67N, 82.40W	1980 to the present	4.0 m	0.6 m
45006 (Superior)	47.34N, 89.79W	1981 to the present	4.0 m	0.6 m
45007 (Michigan)	42.67N, 87.03W	1981 to the present	4.0 m	0.6 m
45008 (Huron)	44.28N, 82.42W	1981 to the present	4.0 m	0.6 m
45012 (Ontario)	43.62N, 77.41W	2002 to the present	4.0 m	0.6 m

^a T_{air} height is the location of the air temperature measurement on the tower or buoy; the depth of the subsurface temperature measurement is given by T_{soil} and T_{lake} for towers and buoys, respectively. Tower and buoy data come from the FLUXNET database and the NOAA National Data Buoy Center (NDBC), respectively. Towers are located at the University of Michigan Biological Station (UMB), Willow Creek (WCr), and Sylvania Wilderness Area (Syv) forest sites. Tower and buoy locations are shown in Figure 1b.

Data from the FLUXNET database [Baldocchi et al., 2001], a cooperative program that compiles data from an international network of flux tower facilities, are used to evaluate soil and air temperature, atmospheric moisture, and evapotranspiration rates. Our analysis domain (GLW) contains 21 FLUXNET locations; however, only three sites (Table 1 and Figure 1b) contain more than 1 year of postprocessed data within the simulation time frame for the variables explored in this study: (1) University of Michigan Biological Station (UMB) [Schmid et al., 2003] in Pellston, MI, (2) Willow Creek (WCr) [Cook et al., 2004] in Park Falls, WI, and (3) Sylvania Wilderness Area (Syv) [Desai et al., 2005] in Watersmeet, MI. All three sites consist of deciduous broadleaf vegetation with subtle differences in species composition. The midsuccessional UMB forest consists of an overstory of aspen and birch overlying an understory of white pine, red oak, and sugar maple [Pressley et al., 2005]. In contrast, Willow Creek contains sugar maple, basswood, and green ash [Cook et al., 2004], and Sylvania Wilderness Area contains eastern hemlock, sugar maple, and birch [Desai et al., 2005]. These species are well represented in the model land cover description, as indicated by the PFTs prescribed in RegCM at the grid points corresponding to the three sites (Table 2). Observed latent heat flux is calculated from eddy covariance measurements of vertical velocity and moisture perturbations ($w'q'$) and compared with modeled evapotranspiration. When comparing with gridded model (section 2.1) and

Table 2. Percentage of the Plant Functional Types (PFT) Prescribed in the RegCM Simulations for the Three FLUXNET Sites: University of Michigan Biological Station (UMB), Willow Creek (WCr), and Sylvania Wilderness Area (Syv)^a

	UMB	WCr	Syv
Needleleaf evergreen temperate tree	16	18	15
Needleleaf evergreen boreal tree	0	1	11
Broadleaf deciduous temperate tree	38	35	19
Broadleaf deciduous boreal tree	0	1	15
C3 nonarctic grass	27	14	29
Corn	18	31	12

^aValues are spatial averages over a 3-by-3 grid (excluding lake points) centered on each flux tower (see geographical coordinates in Table 1).

reanalysis (section 2.3) data sets, we average the gridded data over a 3-by-3 (225 km²) grid centered on the geographical coordinates of each tower (Table 1). Due to its nearby proximity to Lakes Michigan and Huron, the 3-by-3 grid centered on the UMB site contains lake points that we exclude from our analysis over land due to the contrasting nature of land- and lake-atmosphere feedbacks.

In light of the relatively small footprint that tower data covers, we also evaluate evapotranspiration with

remotely sensed observations from the Moderate Resolution Imaging Spectroradiometer (MODIS). We utilize monthly average MODIS evapotranspiration estimated using the Penman-Monteith relationship [Mu *et al.*, 2011]. Because MODIS evapotranspiration data are only available from 2000 onward, our evaluation is limited to years that coincide with the model simulations (2000–2002).

We use buoy-based observations (Table 1) from the NOAA National Data Buoy Center (NDBC) to evaluate climatological lake and surface air temperatures. Each lake contains one to three buoys (Figure 1b) with air and lake surface measurements ranging from 3.2 to 4 m above the lake surface and 0.6 to 1 m below the surface, respectively. We compute a climatological average of the nine midlake buoys (Figure 1) for comparison against lake model grid points. Date ranges for the climatological averages vary due to data availability (Table 1). Buoy stations are typically removed from the lakes over the winter to prevent ice-related damage, leading to reduced data during winter and spring. Therefore, we only show months when less than 10% of the data are missing (June–October).

To supplement the limited buoy-based observations, we also include satellite estimates of lake surface temperature from the NOAA Great Lakes Environmental Research Laboratory (GLERL) Great Lakes Surface Environmental Analysis (GLSEA) data set (1994 to present). This data set offers a more complete picture of LSTs relative to the NCDC buoys, which are point measurements that are valid only during the warm season. Like the MODIS data set, GLSEA is a recent satellite-derived product, and we compare the available data with the simulation years, which overlap from 25 October 1994 to 31 December 2002. To evaluate RegCM-simulated lake evaporation, our analysis uses estimates from the NOAA GLERL hydrologic model, which derive from the Great Lakes Evaporation Model of Croley [1989].

2.3. Reanalysis Products

We supplement the observational data sets with reanalysis products, which assimilate a suite of observational data into global and regional models to create a spatially and temporally continuous atmospheric data set. Here we use evaporation (land, including transpiration, and lake) and upper level atmospheric moisture and winds from the NARR [Mesinger *et al.*, 2006] and ERA [Dee *et al.*, 2011] reanalysis products. Comparing the global ERA reanalysis product with the RCM-ERA simulation allows us to distinguish the influence of the regional model from the lateral boundary conditions. LSTs in NARR are provided by the Great Lakes Environmental Research Laboratory (GLERL), which are in part derived from climatological values. ERA LSTs derive from the NCEP 2-D-Var data set before July 2001 and the NOAA OISST data set after July 2001.

2.4. Precipitation Recycling

To quantify the role of the land and lake surfaces in the Great Lakes hydroclimatology as estimated by reanalysis and RegCM, we estimate the fraction of precipitation that derives from evaporation (P_E/P), or the “moisture recycling efficiency,” using the following relationship [Brubaker *et al.*, 1993; Eltahir and Bras, 1994, 1996; Schär *et al.*, 1999; Zangvil *et al.*, 2004]:

$$\frac{P_E}{P} = \frac{E}{E + IF} \quad (1)$$

where E is the GLW average evapotranspiration (equation (2)) and IF is the advective moisture inflow into the region through the perimeter of the GLW analysis domain outlined in Figure 1b (equation (3)). The validity of equation (1) requires that water vapor deriving from local evaporation and horizontal transport be well mixed in the atmosphere, a condition that studies generally consider met as a result of efficient turbulent transport of evaporated moisture [Budyko, 1974]. E is diagnostically computed as a function of the prognostic specific humidity gradient between the soil and canopy surfaces (q_{sfc}) and the overlying atmosphere (q_a), which is related to the gradient between the vapor pressure of air (e_a) and the saturation vapor pressure of the surface ($e_s(T_{sfc})$):

$$E = -\rho \frac{(q_a - q_{sfc})}{r_{aw}} = \frac{\rho c_p}{\gamma \lambda} \frac{(e_s(T_{sfc}) - e_a)}{r_w} \quad (2)$$

where ρ is the density of the atmosphere, r_{aw} is the bulk aerodynamic resistance of the surface caused by vegetation and the frictional effects of the ground, c_p is the specific heat capacity of dry air at constant

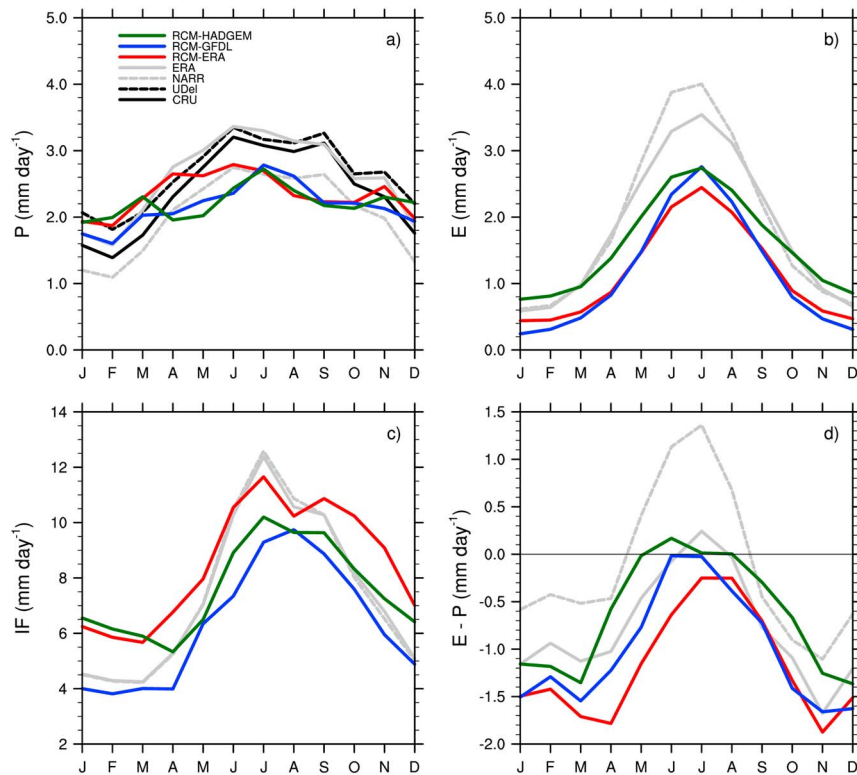


Figure 2. Seasonal climatology (1980–2002) of monthly GLW average (a) precipitation, (b) evaporation, (c) advective inflow (equation (3)), and (d) moisture deficit ($E - P$) in mm d^{-1} for CRU (black solid) and UDel (black dashed) observations (precipitation only), NARR (dashed grey), ERA (solid grey), RCM-ERA (red), RCM-GFDL (blue), and RCM-HADGEM (green). Spatial averages consist of the full GLW domain, including both land and lake grid points.

pressure, γ is the psychrometric constant, λ is the latent heat of vaporization ($2.5 \times 10^6 \text{ J kg}^{-1}$), and r_w is the resistance accounting for surface dryness. Land evaporation comprises soil evaporation, evaporation from interception storage, and transpiration from vegetation foliage. Lake evaporation follows a similar expression as equation (2), only with a weaker drag coefficient. IF is derived using the relationship for moisture flux divergence given by Zangvil *et al.* [2004]

$$IF = OF - \frac{1}{g} \int_{p_t}^{p_s} \oint q V_n dl dp \quad (3)$$

where OF is the flow out of the side boundaries, g is gravity, q is the specific humidity at each boundary, V_n is the wind orthogonal to the respective boundary, p_s and p_t are the surface and top-of-atmosphere pressure, respectively, and dl is the length of the boundary.

By the conservation of mass, the moisture change within the GLW analysis domain ($\partial q / \partial t$) is equal to the sum of the sources and sinks through the surface and side boundaries:

$$\frac{\partial q}{\partial t} = E - P + IF - OF \quad (4)$$

Assuming the moisture tendency ($\partial q / \partial t$) to be negligible for monthly timescales, the moisture deficit ($E - P$) can be used to approximate the net loss through the side boundaries via advection ($OF - IF$), which denotes the moisture flux divergence.

3. Evaluation of Great Lakes Hydroclimate

In this section, we evaluate the hydroclimate of the GLW region with a three-member ensemble of RegCM simulations driven by different lateral boundary conditions. Unless stated otherwise, we present 23 year (1980–2002) seasonal climatologies, averaged spatially over the GLW analysis domain ($40\text{--}50^\circ\text{N}$, $95\text{--}75^\circ\text{W}$, Figure 1b).

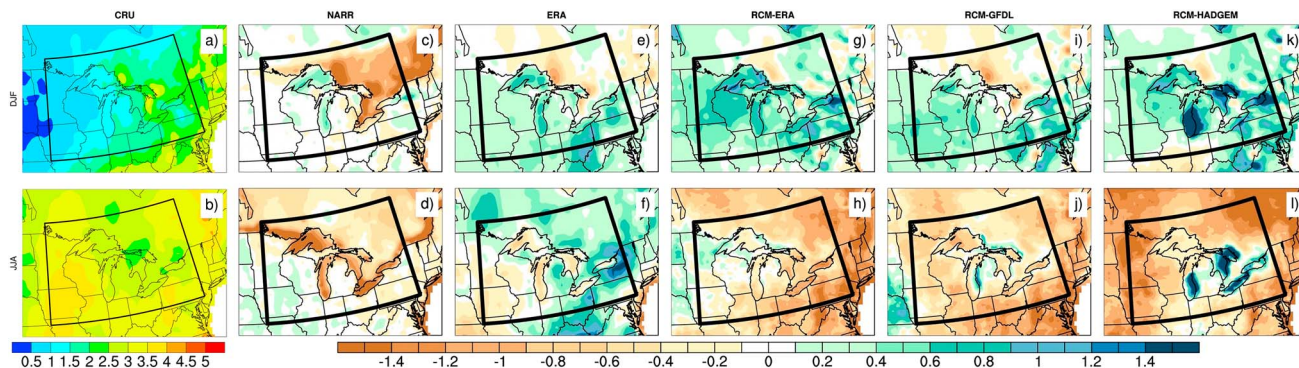


Figure 3. The 1980–2002 climatological average (a, c, e, g, i, and k) winter (DJF) and (b, d, f, h, j, and l) summer (JJA) spatial distribution of observed precipitation (CRU (Figures 3a and 3b); mm d^{-1}) and biases (mm d^{-1}) produced by NARR (Figures 3c and 3d), ERA (Figures 3e and 3f), and RegCM simulations (Figures 3g–3l). Yellow and brown indicate a dry bias relative to CRU; green and blue indicate wet biases.

3.1. Precipitation

Observed precipitation (CRU and UDel) in the GLW region exhibits a seasonal cycle with a winter (December–January–February (DJF)) minimum climatological rate of 1.4 mm d^{-1} and a summer (June–July–August (JJA)) maximum of 3.2 mm d^{-1} (Figure 2a). Both reanalysis products and all model simulations generally capture the seasonal trend but show discrepancies with the observed amplitude. The NARR product underestimates precipitation year round with biases of up to 14 and 24% in summer and winter, respectively. *Li et al.* [2010] found that NARR predicts a band of reduced precipitation along the U.S.–Canada border during the summer caused by discrepancies between U.S.– and Canada-based observational data sets. Using the observations, we confirm that NARR underpredicts summer precipitation not only along the border but also over the Great Lakes (Figure 3d). In winter, a related dry bias occurs between the Canadian shoreline of the Great Lakes and the 49th parallel (Figure 3c). Unlike NARR, the global ERA product overestimates precipitation in the winter, spring, and summer by as much as 22% (Figure 2a). Winter biases are strongest due to the combined contribution of land and the Great Lakes (Figure 3e), whereas dry biases over the lakes balance with wet biases over the surrounding land in summer (Figure 3f).

Relative to the observations and the reanalysis products, all three RegCM simulations have a weaker seasonal precipitation cycle with an average wet bias of up to 31% in winter and a dry bias of up to 21% in summer (Figure 2a; see discussion in section 3.3), suggesting that the regional model may better explain the biases than the driving reanalysis and GCMs. Precipitation gauges may underestimate snowfall due to wind undercatch, which may explain the winter wet bias in the model. The UDel data set corrects for this scaling factor and consequently reduces the winter wet bias. Comparisons of probability distribution functions with the CPC observations (not shown) reveal that the model does not fully capture the observed daily rainfall intensity, leading to the summer dry bias. The biases are consistent over land and lakes in both seasons (Figures 3g–3l) except for strong wet biases over southern Lake Michigan and Lakes Huron, Erie, and Ontario in the RCM-HADGEM simulation (Figures 3k–3l), owing to lake-surface-temperature-induced biases in evaporation (see discussions in sections 3.2 and 4.3). RCM-ERA simulates a weaker seasonal precipitation cycle relative to the parent model (i.e., the global ERA product), mostly on account of the summer dry bias, indicating that the model physics within RegCM accounts for the summer precipitation bias rather than the boundary conditions. To identify the processes responsible for the precipitation biases, we evaluate the moisture sources to the region via evaporation and advection in sections 3.2 and 3.3 below.

3.2. Evaporation

The NARR and ERA reanalysis products estimate GLW average summer evapotranspiration peaks of 4 and 3.5 mm d^{-1} , respectively, and winter minima of 0.6 mm d^{-1} (Figure 2b). RegCM captures the seasonal trend but peaks 41 and 29% lower than NARR and ERA, respectively, on average across the three simulations in the summer. Land evapotranspiration reflects the GLW average (i.e., combined land and lake) seasonal cycle with a maximum in the summer (Figure 4a) due primarily to transpiration from the canopy followed by soil evaporation (not shown). Satellite-observed land evapotranspiration measurements from the MODIS show a summer peak evapotranspiration rate of 3.4 mm d^{-1} , which is 18% higher than RegCM simulations and

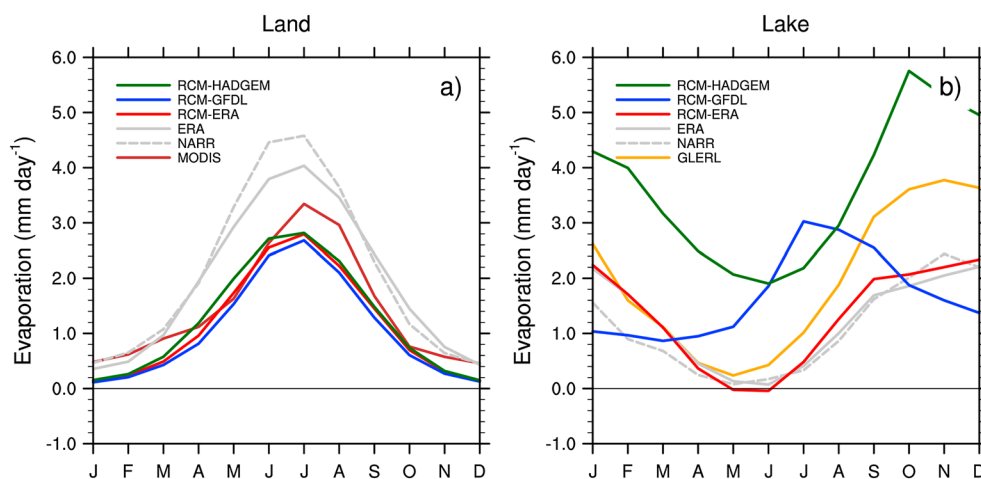


Figure 4. Seasonal climatology (1980–2002) of monthly average evaporation (mm d^{-1}), averaged spatially over the (a) land and (b) lake points within the GLW domain, for MODIS (brown, land only), GLERL (orange, lake only), NARR (dashed grey), ERA (solid grey), RCM-ERA (red), RCM-GFDL (blue), and RCM-HADGEM (green).

18 and 35% lower than ERA and NARR, respectively. On average throughout the year, RegCM shows better agreement with MODIS observations than the reanalyses, particularly during the transition seasons.

Latent heat fluxes measured by eddy covariance at the three FLUXNET stations show that all three RegCM simulations reproduce observed seasonal cycle and magnitude at the WCr and Syv FLUXNET site (Figures 5b and 5c), whereas NARR and ERA overestimate observations at all three sites by a factor of approximately 1.5 and 2, respectively. *Sheffield et al.* [2012] find similar overestimates (28% annually) by the NARR product, and *Ruane* [2010] notes that NARR evapotranspiration is too intense. Midsummer evapotranspiration rates observed at the UMB site (Figure 5a) peak 24–34% higher than at the two Wisconsin-based sites, potentially due to differences in soil moisture content, though soil moisture data are unavailable at UMB during this time period. Neither RegCM nor the reanalyses capture the enhanced evapotranspiration at UMB. These results show that the model land surface in RegCM more closely simulates observed evapotranspiration than the reanalyses, although both struggle to capture the variability across the three observation sites. As noted by previous studies [e.g., *Trenberth and Guillemot*, 1998], the evapotranspiration estimates in the reanalysis products are poorly constrained and model dependent. *Oleson et al.* [2008] note several improvements to land-based evapotranspiration in version 3.5 of CLM relative to its predecessors that may explain the improved performance of RegCM at the WCr and Syv sites. We note, however, that uncertainties in the eddy covariance measurement of evapotranspiration (ranging from 7–12% [*Baldocchi*, 2003] to 40%

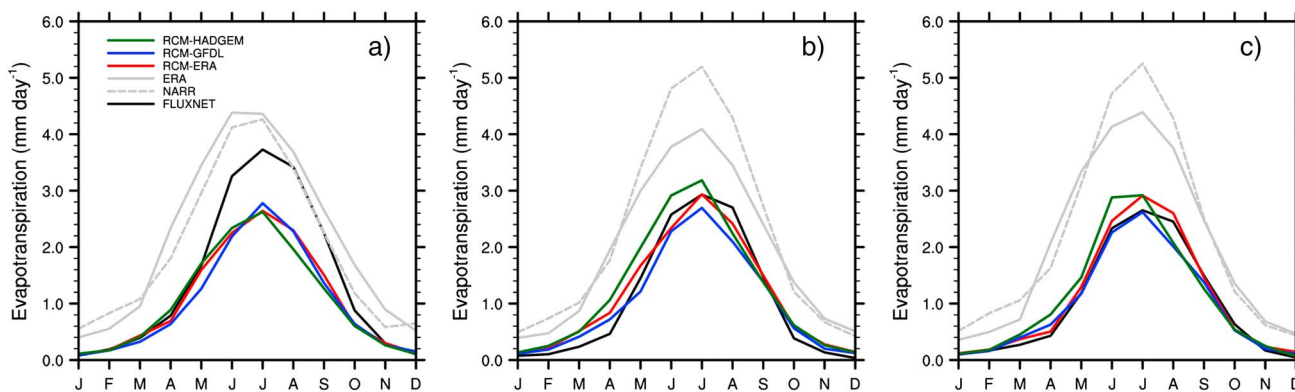


Figure 5. Seasonal climatology of evapotranspiration (mm d^{-1}) at the (a) UMB (1999–2002), (b) WCr (1999–2002), and (c) Syv (2001–2002) tower locations. Point-based observations (black) are shown with simulated spatial averages of a 3-by-3 grid (excluding lake points) centered on the tower coordinates (Table 1) for NARR (dashed grey), ERA (solid grey), RCM-ERA (red), RCM-GFDL (blue), and RCM-HADGEM (green).

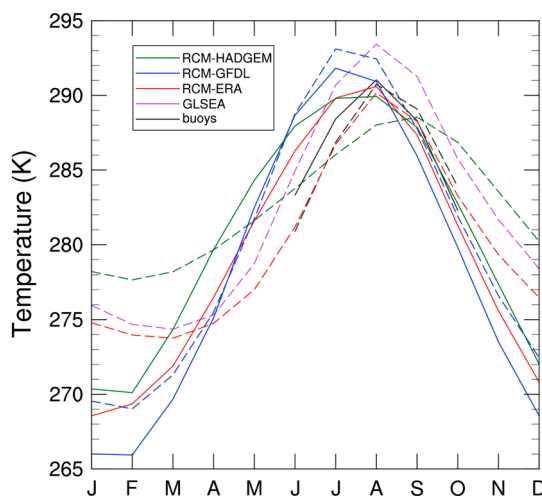


Figure 6. Seasonal climatologies (1980–2002) of air (solid) and lake (dashed) surface temperatures observed by NDBC buoys (black) and NOAA polar-orbiting satellite (GLSEA, 25 October 1994 to 31 December 2002, dashed purple) and simulated by RCM-ERA (red), RCM-GFDL (blue), and RCM-HADGEM (green). Observed values are averaged across all nine buoys (Table 1 and Figure 1b) for the months in which < 10% of the data is missing (June–October). GLSEA is averaged spatially over all five lakes. Simulated values are averaged spatially over the model lake points.

peaks 4 months after land evaporation at 4 mm d^{-1} (Figure 4b). NARR, ERA, and RCM-ERA compare well with the GLERL estimates during the late winter and early spring with respect to both phase and magnitude. From the beginning of summer to midwinter, these products underestimate the estimates from GLERL by as much as 50%. While RCM-ERA resembles the reanalyses, RCM-HADGEM simulates 2–3 times higher lake evaporation than the reanalyses (Figure 4b), and the RCM-GFDL simulation exhibits a seasonal cycle that is shifted in phase. Despite the fact that the lakes make up only 11.8% of the domain, the variability in lake evaporation across the three simulations is evident in the GLW average evaporation (Figure 2b), particularly in the winter when land contributions are small.

To explain the differences in lake evaporation across the three models, particularly the biases in the GCM-constrained simulations, we evaluate the simulated lake and air temperatures with buoy observations and the model-derived GLSEA data (Figure 6). June–October buoy measurements show that LSTs generally follow the air surface temperature seasonal cycle with a 2–3 week lag in warming and cooling during the transition seasons (e.g., March–April–May (MAM) and September–October–November (SON)). The lake surface exerts a strong influence on the surface air temperature measurement, and thus, LSTs may lag behind air temperatures farther than the buoy data suggest, particularly higher in the atmosphere. In addition, the offset seasonal cycle is more apparent when November–May data are included (not shown). GLSEA June–October temperatures show a similar phase as the buoy measurements with 3 K warm biases in the summer and a winter minimum temperature of 275 K. We note, however, that the buoys only capture the deep, midlake conditions while the GLSEA data also include the warm shallow waters and thus appear warmer than the buoys. RCM-ERA captures the GLSEA LSTs in winter and buoy lake and air temperatures in summer, demonstrated by the agreement in lake–air temperature differences (Figures 7a and 7b) and evaporation rates (Figure 4b). In RCM-GFDL, LSTs follow air temperatures, leading to weak lake–air temperature differences year round and a weak seasonal offset in evaporation. RCM-HADGEM LSTs are 8 K warmer than the overlying air in winter and 3 K cooler in summer, leading to a stronger temperature gradient and evaporation rates that are twice that of the other two simulations. We note that these biases are computed from spatial averages across all five lakes and that each lake exhibits strong individual variability, particularly in the RCM-HADGEM case (Figures 7a and 7b), as discussed in section 4.3.

[Vickers *et al.*, 2010]) and soil water limitations on evapotranspiration may also lead to observation–model discrepancies. In addition, tower-based point measurements may not be representative of a 25 km model grid cell due to their relatively small footprint (e.g., 100–200 m at UMB) [Pressley *et al.*, 2005]. Therefore, heterogeneities in the landscape may partially explain discrepancies between the observed and modeled data.

Lake evaporation lags land evapotranspiration due to the high heat capacity of water, as shown in previous modeling studies [Lofgren, 1997] and eddy covariance measurements from midlake islands and lighthouses [Blanken *et al.*, 2011]. In fall and winter, LSTs are warmer than the overlying air, which raises vapor pressure deficit (VPD) and induces lake evaporation (Figure 4b). In contrast, cool LSTs suppress evaporation in the spring and summer by stabilizing the atmosphere. Estimates of lake evaporation from the Great Lakes Evaporation Model from NOAA GLERL averaged spatially over the five lakes demonstrate this offset seasonal cycle that

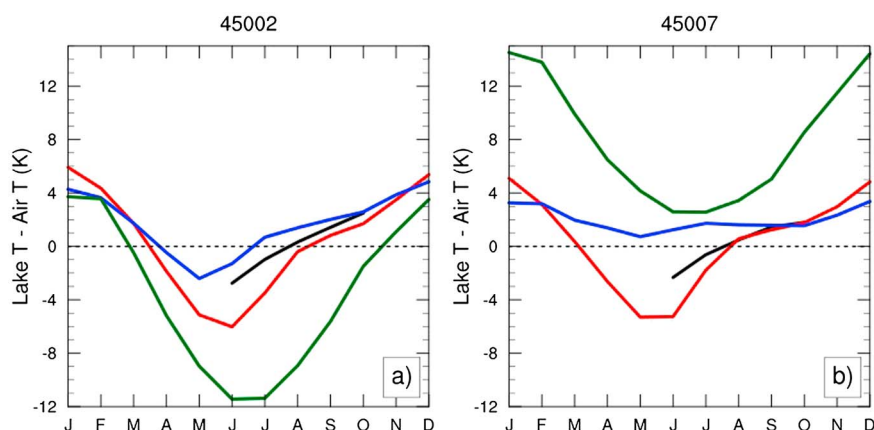


Figure 7. Climatological lake-air temperature gradient for the (a) northern (buoy 45002; 1980–2002) and (b) southern (buoy 45007; 1981–2002) regions of Lake Michigan.

3.3. Moisture Transport

In addition to evaporative sources, precipitation also derives moisture from outside the GLW region via advection. Here we focus on the flow into the GLW region through the lateral boundaries (IF, equation (3)) as it is utilized in the precipitation recycling estimate (equation (1)). IF has a distinct seasonal cycle that peaks in the late summer (Figure 2c). NARR and ERA show nearly identical seasonal cycles with a summer peak near 12.5 mm d^{-1} , decreasing to 4.5 mm d^{-1} in the winter. The agreement between the reanalyses highlights the similarities between the assimilated temperature, wind, and moisture fields in the two data sets. On average across the three model simulations, RegCM estimates a 17% lower July peak inflow rate than the reanalyses with the GCM-driven simulations exhibiting the greatest discrepancies. In the winter, RCM-ERA and RCM-HADGEM advect 23–29% more moisture into the region than the reanalyses, particularly through the southern boundary (not shown), whereas RCM-GFDL simulates 10–11% less. For RCM-ERA, the summer and winter extremes in modeled precipitation are 13% lower and 30% higher, respectively, than CRU and UDel observations (Figure 2a), whereas the IF biases relative to NARR and ERA are 8% lower in summer and 45% higher in winter (Figure 2c). This suggests that IF bias only partially explains the summer dry bias, whereas the high winter IF bias likely drives the wet bias, particularly considering the weak evaporation bias in winter (Figure 2b). In addition, the spread across the model members indicates the influence of synoptic conditions on external moisture sources, such as the pattern and position of the jet stream and placement of high- and low-pressure centers.

To illustrate the influence of synoptic weather patterns on regional moisture inflow, we identify the dominant moisture sources that control IF in the GLW region and compare the variability in moisture source across the three simulations. RCM-ERA captures the dominant flow patterns and moisture sources typically observed in the winter and summer [Mo *et al.*, 2005]. In winter (Figure 8a), the polar jet stream moves southward, transporting cold, dry air to the upper Midwestern U.S. from the northwest. In summer (Figure 8b), significant moisture is transported from the south via the Great Plains low-level jet (LLJ). These seasonally contrasting flow patterns explain the precipitation (Figure 2a) and inflow (Figure 2c) that characterize a wet summer and dry winter climate.

In contrast with RCM-ERA, RCM-GFDL simulates approximately 30% less moisture in the northwest in winter (Figure 8c) and nearly 25% less in the western Gulf of Mexico in summer (Figure 8d) at 850 hPa. In addition, RCM-GFDL simulates weaker zonal winds at 850 hPa, signified by easterly wind vectors along the U.S.–Canada border in Figure 8b. Both the weaker upstream moisture availability and winds contribute to reduced IF year round in RCM-GFDL relative to RCM-ERA (Figure 2c), resulting in up to 15% less atmospheric moisture in the GLW domain. Sheffield *et al.* [2013] examine moisture transport in North America, simulated by the GFDL-ESM2M parent model (among other CMIP5 models), and find similar large-scale patterns in winter and summer as simulated here. Like RCM-GFDL, RCM-HADGEM simulates less moisture in the northwest and southern winter and summer moisture sources than RCM-ERA (Figures 8e and 8f), which promote IF reductions, as seen in summer (Figure 2c). In the winter, however, the reduced availability in

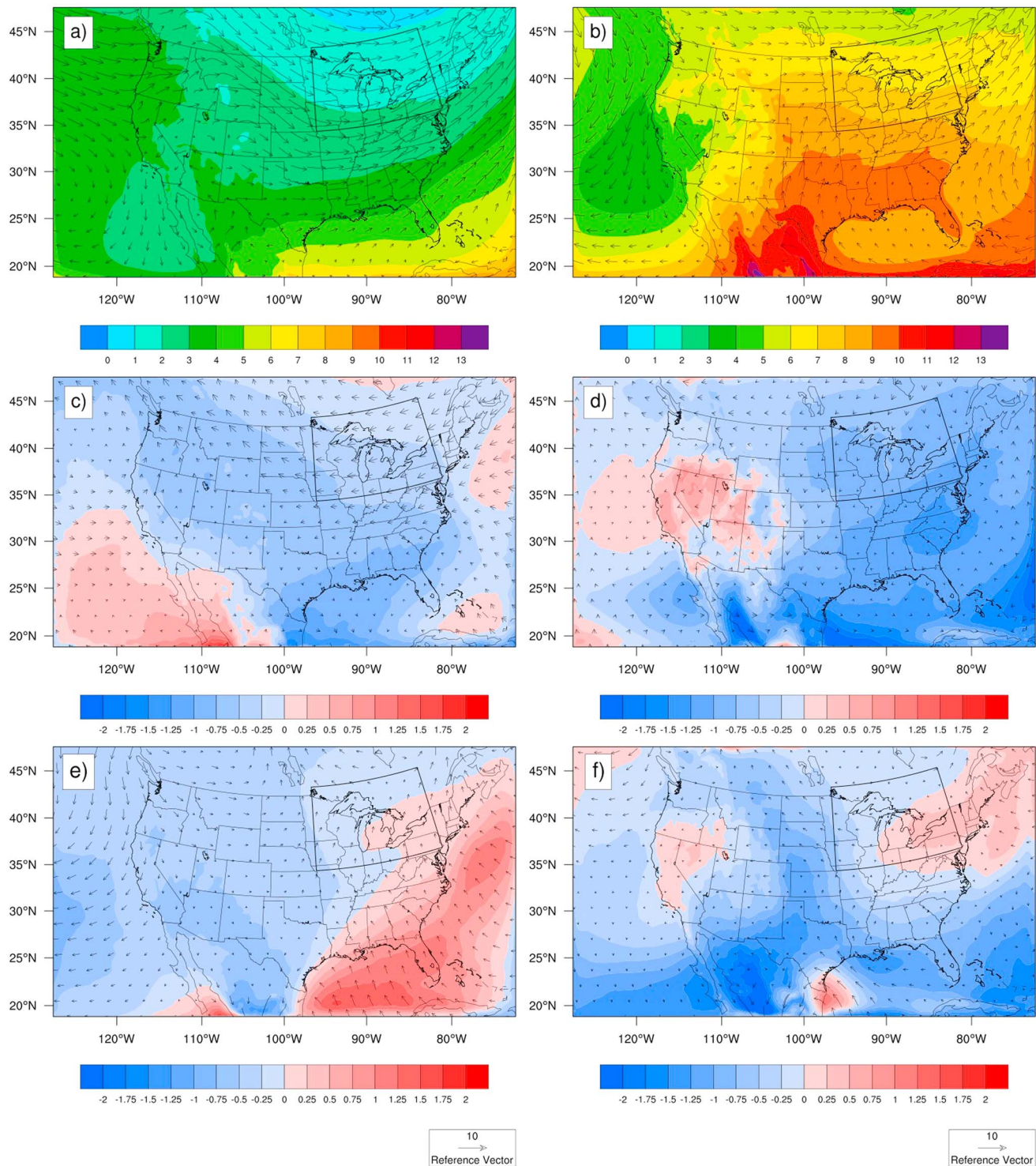


Figure 8. Twenty-three year (1980–2002) climatological average (a, c, and e) winter (DJF) and (b, d, and f) summer (JJA) 850 hPa specific humidity (g kg^{-1} , colored contours) and winds (m s^{-1} , vectors) for RCM-ERA (Figures 8a and 8b) and the differences between RCM-ERA and RCM-GFDL (Figures 8c and 8d) and RCM-HADGEM (Figures 8e and 8f). In the difference plots (Figures 8c–8f), RCM-ERA is subtracted from the GCM-constrained simulations. Red and blue designate more and less moisture, respectively, relative to RCM-ERA. Vectors in Figures 8c–8f represent the change in wind speed between RCM-ERA and the GCM-driven simulations, so vectors oriented toward the west indicate weaker westerly winds or stronger easterly winds.

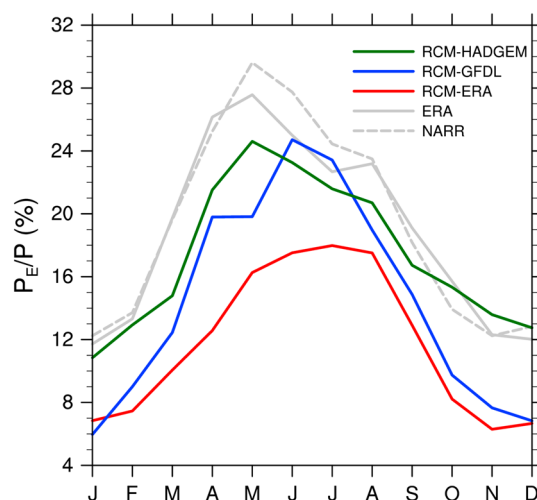


Figure 9. As in Figure 2 but for the moisture recycling efficiency (equation (1)).

upstream moisture, which is less substantial than in RCM-GFDL, is balanced by enhancements caused by increased southerly flow (Figure 8e), leading to similar inflow rates as RCM-ERA (Figure 2c).

Both GCM-driven simulations exhibit lower IF in the summer due to reduced moisture in the LLJ region, where other studies identify challenges simulating convective precipitation. *Dai et al.* [1999] found that when driven by three convection schemes including the Grell scheme used in the present study, RegCM simulates the onset of moist convection and thus convective precipitation too readily. Consequently, the atmospheric moisture and convective energy generated over the Rocky Mountains are depleted over the Great Plains resulting in insufficient convective precipitation in the upper Midwest compared to observations. Alternatively, the

model may underestimate the influence of the LLJ on convective cloud formation in the Great Plains [*Ghan et al.*, 1996]. While the spatial resolution used in our study (25 km) is among the highest applied to regional climate model simulations of the continental United States, the resolution is still too low to fully capture the small-scale physics of convection [*Iorio et al.*, 2004]. Overall, our results illustrate that the placement of synoptic features strongly influences the contribution of external moisture sources toward local precipitation, which must be considered when estimating the relative roles of evaporative and advective moisture sources for a given region.

Moisture in the GLW domain exits via advective outflow. By assuming a negligible change in storage of atmospheric moisture within the domain over time at the monthly timescales considered here (i.e., $\frac{\partial q}{\partial t} \approx 0$), we can approximate the net loss (i.e., divergence, $OF - IF$) of atmospheric moisture through the side boundaries by the net gain of moisture from the surface boundary ($E - P$, see equation (4)). The RegCM simulations and ERA reanalyses exhibit a net loss in atmospheric moisture through the surface boundary ($P > E$, Figure 2d) in the winter, drawing inflow to the region through the side boundaries and signifying convergence. In the summer, P approximately balances E , indicating negligible moisture loss or gain. In contrast, NARR estimates half to one third the convergence of the ERA and three RCM simulations in the winter and strong divergence in the summer. The reduced precipitation (Figure 2a) combined with enhanced evaporation (Figure 2b) in NARR during the summer explains the offset from the other simulations in the moisture deficit. Excluding NARR, precipitation exceeds evaporation on average annually, inducing advection and convergence.

4. Assessment of Surface-Atmosphere Feedbacks on Great Lakes Hydroclimate

In this section, we explore how the land and lake surfaces influence the atmosphere and affect Great Lakes hydroclimate feedbacks. First, we quantify the role of the surface sources as a local moisture source for precipitation relative to external, upstream moisture by estimating the efficiency of local moisture recycling (equation (1)). We then assess the ability of the regional climate model to capture the drivers of land-atmosphere and lake-atmosphere feedbacks by comparing simulated conditions and moisture fluxes across the interface against observations from FLUXNET and buoy data (section 2.2).

4.1. Moisture Recycling

The moisture recycling term (P_E/P , equation (1)) is one metric to quantify the feedbacks between the surface and atmosphere. This ratio yields the percentage of precipitation that derives from evaporation. P_E/P peaks in the late spring to midsummer, with NARR and ERA reanalysis estimating annual maxima in May of up to 30 and 28%, respectively, and minima of 12% in winter (Figure 9). Because winter lake evaporation exceeds that from land by up to an order of magnitude (Figure 4), lake feedbacks such as lake-effect snow drive winter recycling. All RegCM members underestimate the recycling ratio estimated by the reanalyses year

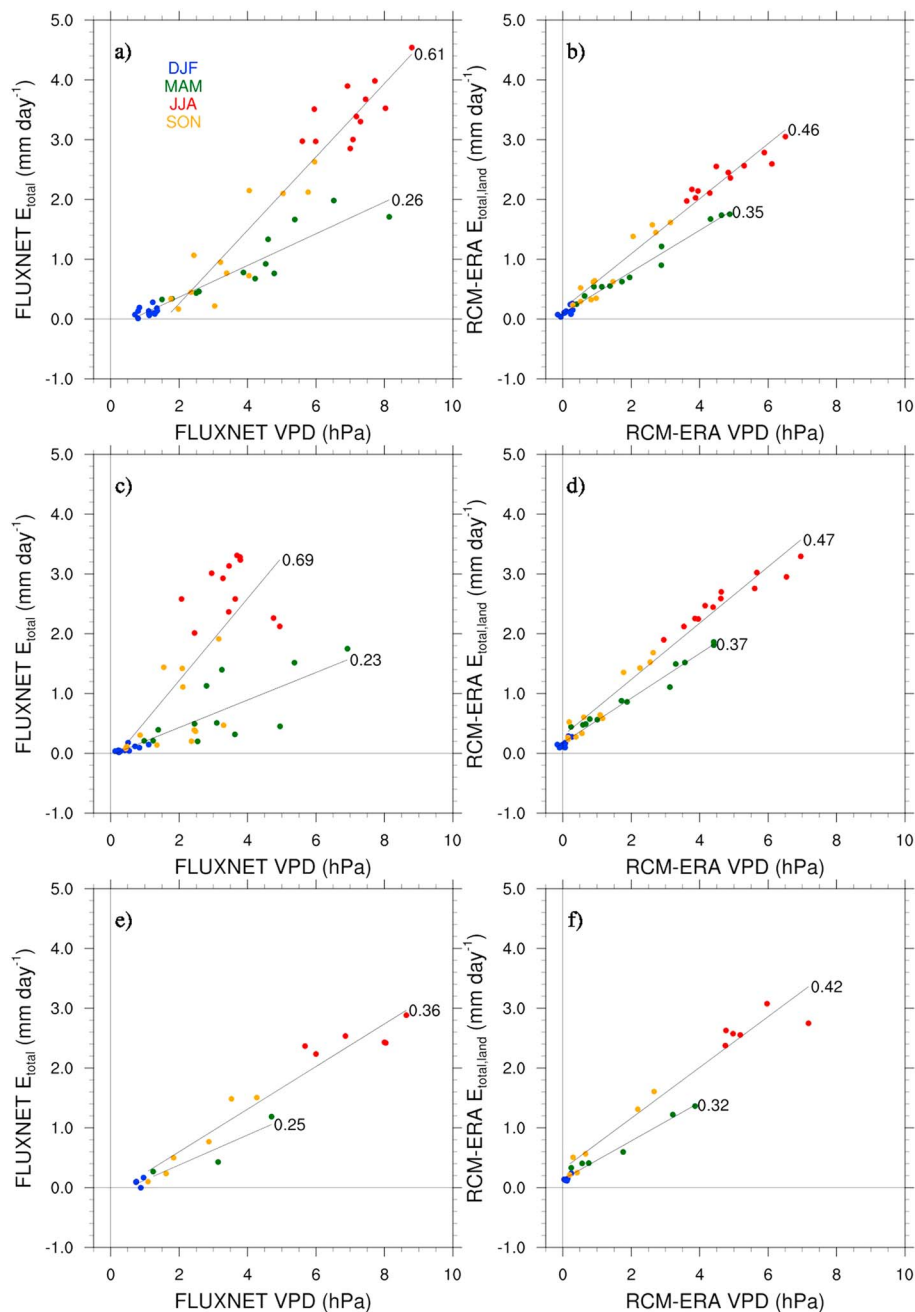


Figure 10. (a, c, and e) Observed and (b, d, and f) simulated (RCM-ERA only, 2 m) monthly average evaporation (mm d^{-1}) with respect to vapor pressure deficit (VPD, hPa) at the UMB (1999–2002 (Figures 10a and 10b)), WCr (1999–2002 (Figures 10c and 10d)), and Syv (2001–2002 (Figures 10e and 10f)) tower locations. Linear regressions and corresponding slopes for the winter-spring and summer-fall seasonal groups are shown in black. Each data point represents a monthly average value for a given year and is color coded by season: spring (MAM) in green, summer (JJA) in red, autumn (SON) in orange, and winter (DJF) in blue.

round, with discrepancies in the summer maximum ranging from 11–21% in the GCM-driven simulations to 49% in RCM-ERA. However, as discussed in section 3.2, the reanalyses overestimate warm season-observed evapotranspiration rates, suggesting the reanalyses recycling ratios are likely overestimated. Because RegCM captures the evaporation at two of the three FLUXNET sites, the model may be the most realistic representation. RCM-ERA estimates the lowest contribution (18% summer maximum) of local evaporation to local precipitation due to the combined effects of lower land evaporation (Figure 4a) and higher

advective inflow (Figure 2c) relative to the other model members. All three simulations, however, exhibit similar evaporation (Figure 2b), and thus, the recycling differences derive from differences in moisture transport (Figure 2c and section 3.3). RCM-ERA recycles 42% less moisture than its global parent product, suggesting that the evaporation and transport discrepancies derive from the effect of dynamical downscaling and varying treatments of atmospheric and land surface processes rather than the boundary conditions. In winter, RCM-HADGEM has evaporation rates (Figure 2b) and thus recycling efficiencies that are twice as high as the other two members due to enhanced lake evaporation (Figure 4b; see discussion in section 4.3). The concurrent enhancement in lake evaporation and precipitation along the shorelines of the Great Lakes in the RCM-HADGEM case (Figures 3k and 3l) illustrates the surface feedbacks on local precipitation.

Despite little evidence of lake feedbacks on summer recycling, our results reveal that the surface contributes up to third of the moisture precipitated locally in the Great Lakes region relative to external sources. While our findings are consistent with studies of other regions, the discrepancies between simulated and reanalysis-estimated evaporation rates identified in section 3.2 suggest that we may underestimate the role of the surface in the Great Lakes region.

4.2. Land-Atmosphere Feedbacks

To understand the control of fluxes from the land surface on the atmosphere, we examine the drivers of surface moisture fluxes based on FLUXNET observations and the RegCM model simulations. As shown by equation (2), evapotranspiration occurs when the moisture content (or vapor pressure) of the surface exceeds that of air. Evapotranspiration is limited by the amount of water vapor the atmosphere can hold; therefore, the vapor pressure deficit of air ($VPD = e_s(T_a) - e_a$) is an effective proxy for evaporative demand. Measurements taken at three FLUXNET sites within the GLW domain show a linear relationship between evaporation and VPD, with evaporation increasing with increasing VPD from winter to summer (Figures 10a, 10c, and 10e). The measurements can be fit with two linear relationships: one for winter and spring and another, with a steeper slope, for summer and fall. This pattern indicates that the evapotranspiration response to VPD is stronger in the summer and fall than in the winter and spring. One likely explanation for this phenomenon is that the cool soils inhibit evaporative fluxes in the winter and spring by lowering the surface saturation vapor pressure and vice versa in summer and fall when the soil surface is warm. All three sites exhibit nearly identical winter-spring slopes ($\sim 0.25 \text{ mm d}^{-1} \text{ hPa}^{-1}$), whereas the summer-fall slope varies from 0.61 and 0.69 $\text{mm d}^{-1} \text{ hPa}^{-1}$ at UMB and WCr, respectively, to 0.36 $\text{mm d}^{-1} \text{ hPa}^{-1}$ at Syv. Like the observations, all model members (Figures 10b, 10d, and 10f; RCM-ERA only shown) exhibit two linear relationships for the winter-spring and summer-fall regimes, where the summer-fall slope exceeds that of the winter-spring relationships; however, the model does not fully capture the magnitude and site-to-site variability in slope. RCM-ERA overestimates the winter-spring slope by 35 and 28% at UMB and Syv, respectively, and by 61% at WCr. In contrast, the model underestimates the summer-fall slope at UMB and WCr by 25 and 32%, respectively, and overestimates the slope at Syv by 17%. While the model captures the site-to-site variability in the winter-spring slope (0.03 $\text{mm d}^{-1} \text{ hPa}^{-1}$ observed versus 0.05 $\text{mm d}^{-1} \text{ hPa}^{-1}$ simulated), the model displays insufficient across-site variability in the summer-fall seasons (0.33 $\text{mm d}^{-1} \text{ hPa}^{-1}$ observed and 0.05 $\text{mm d}^{-1} \text{ hPa}^{-1}$ simulated) when evapotranspiration is the strongest. This lack of variability across the three sites in the VPD-evaporation relationship may account for lack of variability in the summer evaporation peak (section 3.2 and Figure 5) and suggests that the model does not fully capture the dependence of evaporation on VPD.

To more fully understand what drives land evapotranspiration, we examine the controls on VPD. VPD depends exponentially on air temperature through the saturation vapor pressure ($e_s(T_a)$) according to the Clausius-Clapeyron relationship. Like the relationship between VPD and evaporation, VPD and $e_s(T_a)$ show two distinct linear relationships for the winter-spring and summer-fall seasons according to measurements (Figure 11). In this case, however, the winter-spring slope is steeper than the summer-fall slope, indicating a stronger VPD response to air temperature in the winter and spring. As discussed above, evaporative fluxes in winter and spring may be lower than summer and fall due to cooler soils, which leads to drier air and thus enhanced VPD. As with VPD and evaporation, the model does not capture the variability in slopes of the VPD- $e_s(T_a)$ relationship across the three sites. The model shows a range in slope between the sites of 0.06 and 0.03 hPa hPa^{-1} for the winter-spring and summer-fall regimes, respectively, contrasting with the observed ranges of 0.21 and 0.19 hPa hPa^{-1} . While RegCM captures the summer-fall slope at UMB (Figures 11a and 11b) and Syv (Figures 11e and 11f), the model underestimates the winter-spring slope by

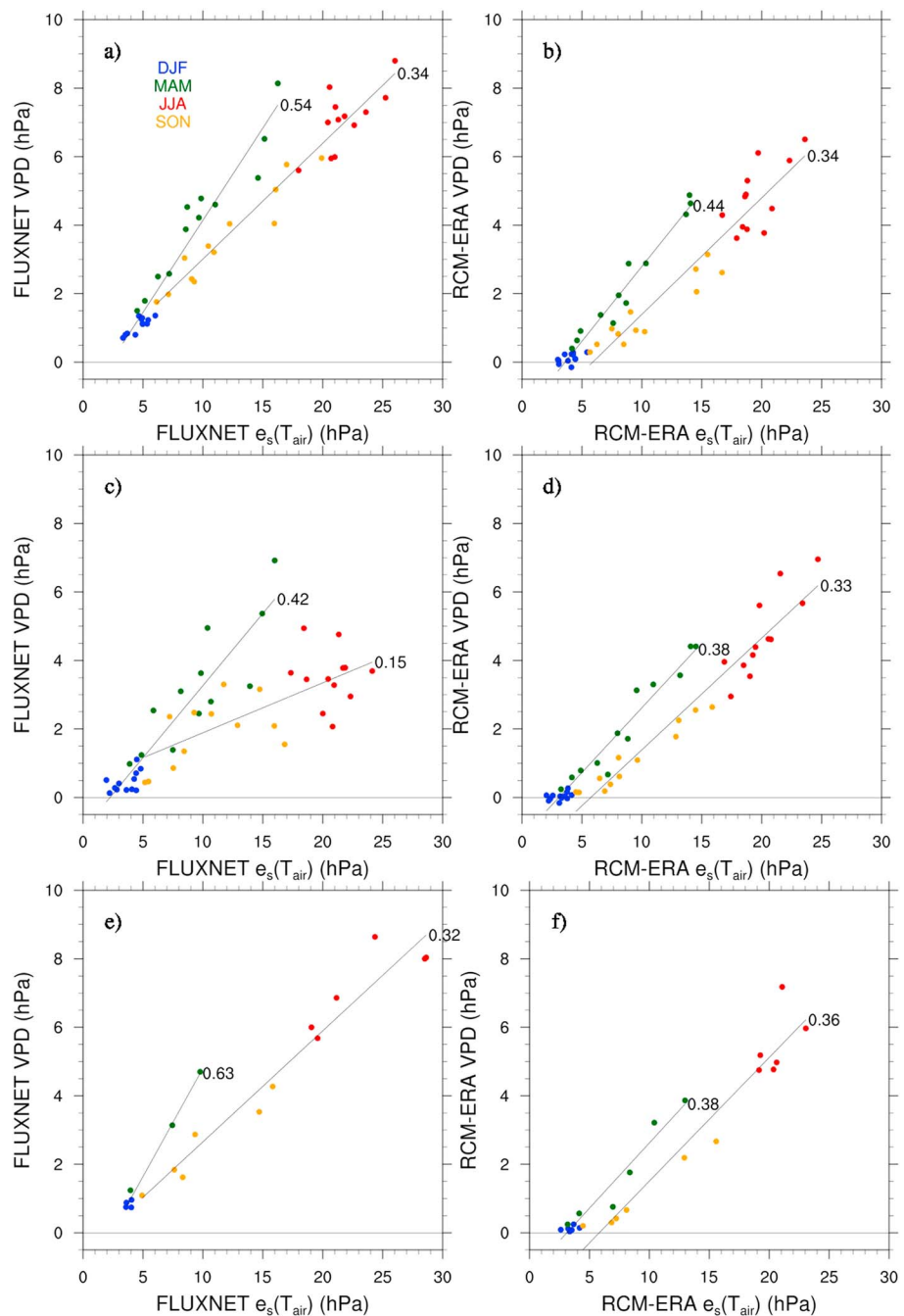


Figure 11. As in Figure 10 but for VPD (hPa) with respect to saturation vapor pressure of air (hPa).

19 and 40%, respectively. At WCr (Figures 11c and 11d), the model underestimates the winter-spring slope by only 10% yet overestimates the summer-fall slope by over a factor of 2. Biases in leaf area could partially explain the across-site variability. Measured leaf area index (LAI) values range from 3.5 to 4.12 $\text{m}^2 \text{m}^{-2}$ at UMB [Pressley *et al.*, 2005; Nave *et al.*, 2011], 5.3 $\text{m}^2 \text{m}^{-2}$ at WCr [Cook *et al.*, 2004], and 4.06 $\text{m}^2 \text{m}^{-2}$ at Syv [Desai *et al.*, 2005], whereas RegCM peak summer LAI values are approximately 4.25, 4.5, and 4.3 $\text{m}^2 \text{m}^{-2}$, respectively. Modeled LAI values show less variability than observed, and this may in part explain the discrepancies between modeled and observed summer-fall slopes. Further, UMB and Syv have similar observed LAI but different observed summer-fall E -VPD slopes (0.61 and 0.36 $\text{mm d}^{-1} \text{hPa}^{-1}$, respectively). This suggests that soil moisture differences may manifest in either canopy transpiration or soil evaporation,

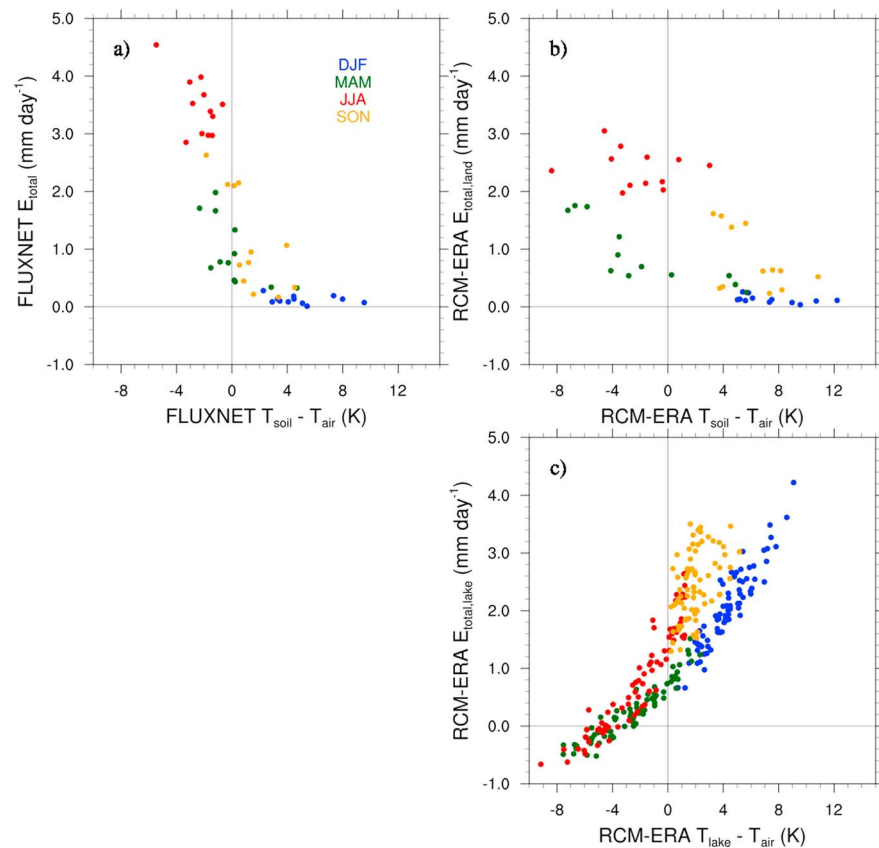


Figure 12. (a) Observed and (b) simulated (RCM-ERA) relationship between monthly average evaporation (mm d^{-1}) and the soil-air temperature difference (K) at UMB (1999–2002); (c) simulated (RCM-ERA) evaporation (mm d^{-1}) with respect to the lake-air temperature difference (K) at the 45007 buoy (1981–2002). Data points represent monthly average values and are color coded by season, as described in Figure 10.

yet this is difficult to evaluate with existing observations. These model-measurement comparisons of both the E -VPD and $\text{VPD}-e_s(T_a)$ relationships suggest that land-atmosphere feedbacks through evaporation and their dependence on atmospheric conditions such as temperature and VPD are not fully captured by the model, in particular the spatial variability of these feedbacks and their response to these atmospheric drivers.

4.3. Lake-Atmosphere Feedbacks

Land and lake evaporation exhibit different relationships with the surface air temperature gradient, suggesting variability in the drivers of these two processes (Figure 12). Observed evaporation over land exhibits an inverse relationship with the soil-air temperature gradient (Figure 12a), likely due to cooler soil temperatures resulting from canopy shading. As warm, unsaturated air passes over a cooler and more moist land surface, surface water evaporates, leading to positive evaporation values. Alternatively, snow cover inhibits evaporation in the winter, while insulating the soil such that temperatures become warmer than air, whereas in the summer, canopy shading leads to cooler soils relative to air. In contrast, simulated lake evaporation is strongly and positively correlated with the air-lake temperature gradient (Figure 12c). As cool air passes over the lake in fall and winter, the warm waters heat the lower atmosphere, which lowers the atmospheric vapor pressure, thus creating a vapor pressure gradient between the lake and lower atmosphere that induces evaporation. These results demonstrate a significant distinction between the forces that drive surface-atmosphere feedbacks over land versus lake surfaces. The model generally captures the relationship over land (Figure 12b); however, we are unable to evaluate the lake evaporation dependence on the surface air temperature gradient due to limited lake evaporation observations during the present simulation period. *Blanken et al.* [2011] confirm the role of near-surface atmospheric vapor

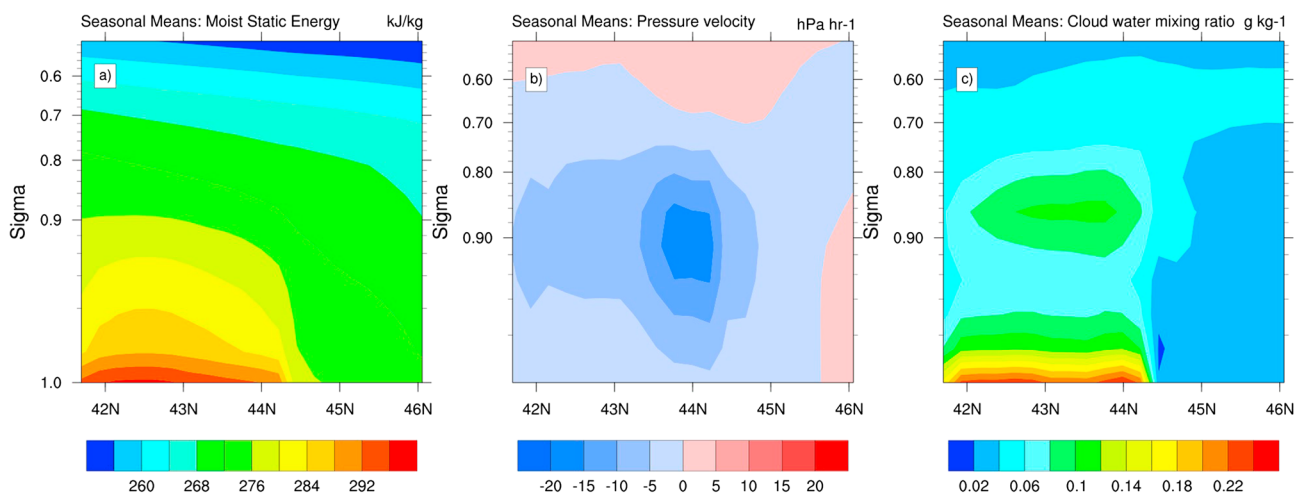


Figure 13. RCM-HADGEM-simulated climatological average winter (DJF) (a) moist static energy (kJ kg^{-1}), (b) pressure tendency (hPa h^{-1}), and (c) cloud water vapor mixing ratio (g kg^{-1}) from the surface ($\sigma = 1$) to approximately 500 hPa ($\sigma = 0.5$) along the transect oriented north-south along central Lake Michigan shown in Figure 1b. Negative pressure tendency (blue) indicates rising motion.

pressure in driving lake evaporation and note surface winds as a secondary driver of evaporation, which is captured indirectly in the model through the drag coefficient.

The RCM-HADGEM member demonstrates the influence of the lakes in modifying local hydroclimate in all seasons. Due to the lack of LST data in the parent HadGEM2-ES model, LSTs are obtained by interpolating between Pacific and Atlantic Ocean SSTs, as well as the Hudson Bay. This approximation yields unrealistic LSTs in the model but also provides a unique opportunity to examine the climate impacts of the lakes under a range of LSTs. An artifact of the HadGEM SST interpolation is that the lakes are split into two regimes with contrasting atmospheric feedbacks: in the northern lakes (northern Lake Michigan and Superior), LSTs are colder than observed (Figure 7a, buoy 45002) and in the southern lakes (southern Michigan, Huron, Erie, and Ontario), LSTs are warmer than observed (Figure 7b, buoy 45007). In the southern lakes, the warm LSTs heat the overlying atmosphere, resulting in enhanced evaporation (Figures 2b and 4b) and moisture recycling (Figure 9). In addition, convection is enhanced over the warm surface waters. This surface effect propagates into the atmosphere via its effect on vertical profiles of moist static energy (MSE), pressure tendency, and cloud water vapor mixing ratios along the N-S cross section of Lake Michigan indicated in Figure 1b

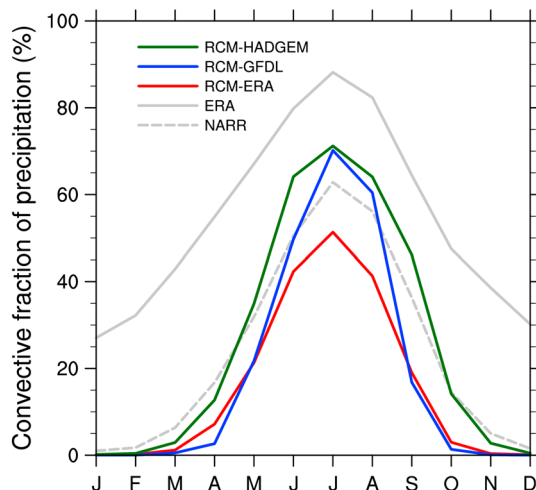


Figure 14. As in Figure 2 but for fraction of precipitation deriving from convection (%).

(Figure 13). Over the southern lakes (near buoy 45007), the higher atmospheric humidity and temperature over the warm lake waters increase the MSE (Figure 13a), which drives convection, as indicated by the enhanced rising motion (Figure 13b). The increased surface humidity and rising motion promote the development of convective clouds above the warm surface waters (Figure 13c). Over the cooler northern lake waters (near buoy 45002), these effects on MSE, vertical velocity, and cloud development are not present. The increased convection over the warm southern waters leads to substantial enhancements in convective precipitation over the lakes and their shorelines downstream (Figures 3k and 3l), which increases the overall convective fraction of precipitation in the Great Lakes region by 7–14% (Figure 14). Overall, we find

that a 4 K increase in LST between the RCM-ERA and RCM-HADGEM simulations in July (Figure 7b) increases convective precipitation by 10% (Figure 14) or a response rate of $2.5\% \text{ K}^{-1}$.

In contrast with the warm southern lake surface waters, the cool northern lake surfaces stabilize the atmosphere and inhibit evaporation. Reduced evaporation minimizes cloud cover over the region, increasing the solar radiation received at the surface (not shown), which also modify surface-atmosphere feedbacks, particularly over the land. Both the warm and cool LST regimes highlight the strong atmospheric feedbacks that can occur due to the lake lower boundary condition and their consequences for variables such as precipitation.

5. Conclusions

Using a regional climate model, we simulate present-day hydroclimate to understand the role of surface-atmosphere interactions on regional precipitation in the Great Lakes region. We perform three simulations with different lateral boundary conditions and lake surface temperatures to identify how atmospheric and surface conditions modify these interactions. By evaluating the model with observations and examining the terms of the moisture budget, we can understand the ability of RegCM to capture regional water cycling. We then examine the feedbacks between the surface and atmosphere and their drivers by analyzing moisture recycling and assessing the model's ability to accurately capture these feedbacks.

Relative to a suite of observational data sets and two reanalysis products, RegCM underestimates the amplitude of the regional hydroclimate. For precipitation, the model simulates wetter winters and drier summers than observed. Evaporation is simulated up to 30–40% lower than the reanalysis products yet is consistent with observations at two FLUXNET stations. However, the reanalyses overestimate evaporation rates at all three sites in the present study by up to twofold, yet neither the model nor the reanalyses capture the spatial variability in evaporation fluxes exhibited by the three sites. We also find that the model underestimates the amplitude of the seasonal cycle of moisture advection into the region as compared to reanalysis, which may contribute to the precipitation biases. Our analysis of the seasonal average synoptic patterns suggests that regional climate models underestimate upstream moisture sources, particularly in the summer in the central Plains and Gulf of Mexico. As earlier studies suggest [e.g., Ghan *et al.*, 1996; Dai *et al.*, 1999; Iorio *et al.*, 2004], improved parameterizations are needed to better capture the onset and frequency of convection generated in the Rocky Mountains and enhance moisture transport into the Great Lakes region via the Great Plains low-level jet.

While precipitation predominantly originates from moisture sources external to the Great Lakes region, the surface can contribute up to 30% of the moisture during the summer and 12% during the winter. The evaporation bias reduces the modeled recycling efficiency of moisture, which suggests that moisture recycling in the Great Lakes region may be more efficient than that estimated by these regional climate model simulations. These results indicate that local feedbacks on regional hydroclimate are not negligible, as previous studies suggest [e.g., Budyko, 1974; Li *et al.*, 2010], and such feedbacks should be considered in future hydroclimate analyses. Comparisons of RegCM driven by ERA reanalysis with the global ERA product indicate that downscaling large-scale boundary conditions and the representation of land surface processes in regional models have a substantial effect on simulated surface-atmosphere feedbacks. Synoptic conditions also modify recycling via their effect on inflow rates.

Land-based evapotranspiration correlates with the vapor pressure deficit, which depends on the temperature and humidity of the lower atmosphere. FLUXNET observations indicate two different linear slopes between the winter-spring and summer-fall VPD-evaporation relationships. In addition, we find that the dependence of evaporation on VPD varies across the three sites. RegCM reproduces the winter-spring slope but does not capture the spatial variability in the summer-fall slope across the observational sites. Similar to the VPD-evaporation relationship, the model captures the dependence of VPD on temperature via the saturation vapor pressure but does not capture the variability in slopes across the three sites. These results show that RegCM does not fully capture the response of evaporation to its atmospheric drivers, in particular the spatial variability in these responses, which may explain the lack of spatial variability in evaporation in the model. Overall, our comparisons with FLUXNET demonstrate that deficiencies in the simulation of surface-atmosphere fluxes still exist despite vast improvements in the representation and treatment of land surface properties and processes in complex land surface models such as CLM. To improve parameterizations of the fundamental surface-atmosphere hydrologic feedbacks, future model

development would benefit from further examination with FLUXNET observations at other regions in effort to develop an improved global characterization of the controls on evaporative demand (e.g., near-surface air temperature).

The Great Lakes also interact with the atmosphere and affect the local hydroclimate. Warm lake surface temperatures can warm and moisten the lower atmosphere, leading to high moist static energy, decreased stability, strong rising motion, and cloud formation, all of which promote enhanced convective precipitation along the downstream shoreline of the lakes. In contrast, cool lake surface temperatures stabilize the atmosphere and inhibit evaporation and subsequent cloud formation, thus allowing greater solar radiation and less precipitation into the surface. Our simulations show that a 4 K bias in lake-air temperature difference in the summer can drive enhanced precipitation along the downstream shoreline by up to 10%. These results indicate the importance of lake temperature on the regional hydroclimate and the necessity to provide accurate lake temperature data for the surface boundary condition in climate models.

Our study contains a few limitations worth noting. First, many of the moisture budget components lack sufficient observational data for evaluating the model. While our evaluation of precipitation and surface energy fluxes has a network of ground-based observations, we rely on model-based reanalysis products to evaluate the other components of the moisture budget (e.g., evapotranspiration and moisture advection), which includes its own uncertainties. In fact, our evaluation indicates that the reanalyses overestimate evapotranspiration at all three FLUXNET sites in our analysis domain. The lack of evaporation measurements over the Great Lakes themselves provides a poor constraint for the models.

In addition to the reanalyses uncertainties, the RegCM hydroclimate variables depend on a number of physical parameterizations. In the results presented here, we focus on the variability that can be introduced by lateral boundary conditions but note that details of the parameterizations chosen may affect our results. For precipitation, we use one convection scheme for simplicity but note that other schemes can provide varying estimates of precipitation.

Finally, while the exclusion of a coupled lake model is justifiable for the purposes of this study, we note that this limits the applicability of our results for future climate projections. Lake models are necessary in downscaled regional climate models to resolve the physical processes affecting the transport of heat within the lake, such as turbulent diffusion and mixing, that large-scale GCMs cannot resolve. While some regional climate model applications utilize a lake circulation model to capture vertical and horizontal mixing [e.g., Yao *et al.*, 2013; Turuncoglu *et al.*, 2013], we did not include these effects in these simulations. Due to poorly simulated ice coverage and relatively high evaporation over ice, lake ice formation is not considered in our simulations, posing a limitation to our analysis of winter lake-atmosphere feedbacks.

In the Great Lakes region, prior studies have shown that synoptic conditions drive the regional hydroclimate. We conclude that while synoptic processes are important climatic drivers in the region, local feedbacks between the surface and atmosphere play an important role in the local hydroclimate. Synoptic conditions can strongly modify surface-atmosphere interactions, and the land and lake surface can modify synoptic conditions to further impact such interactions. Accurate representation of surface-atmosphere interactions and their response to synoptic conditions require careful selection of surface boundary conditions, such as the land surface model and lake temperature specification. Overall, our research highlights the role of the land and lake surfaces on local and regional climate and suggests that further constraints on surface evaporation may improve the representation of these processes in climate models.

References

- Baldocchi, D., et al. (2001), FLUXNET: A new tool to study the temporal and spatial variability of ecosystem-scale carbon dioxide, water vapor, and energy flux densities, *Bull. Am. Meteorol. Soc.*, 82(11), 2415–2434.
- Baldocchi, D. D. (2003), Assessing the eddy covariance technique for evaluating carbon dioxide exchange rates of ecosystems: Past, present and future, *Global Change Biol.*, 9(4), 479–492.
- Bates, G. T., F. Giorgi, and S. W. Hostetler (1993), Toward the simulation of the effects of the Great Lakes on regional climate, *Mon. Weather Rev.*, 121(5), 1373–1387.
- Bates, G. T., S. W. Hostetler, and F. Giorgi (1995), Two-year simulation of the Great Lakes region with a coupled modeling system, *Mon. Weather Rev.*, 123(5), 1505–1522.
- Blanken, P. D., C. Spence, N. Hedstrom, and J. D. Lenters (2011), Evaporation from Lake Superior: 1. Physical controls and processes, *J. Great Lakes Res.*, 37(4), 707–716.
- Bonan, G. B. (2008), Forests and climate change: Forcings, feedbacks, and the climate benefits of forests, *Science*, 320(5882), 1444–1449.
- Brubaker, K. L., D. Entekhabi, and P. S. Eagleson (1993), Estimation of continental precipitation recycling, *J. Clim.*, 6(6), 1077–1089.
- Budyko, M. I. (1974), *Climate and Life*, 508 pp., Academic Press, Orlando, Fla.

Acknowledgments

Funding for this work was provided by the National Science Foundation under grant 1039043. Funding for UMB tower research was provided by the U.S. Department of Energy, Office of Science. Funding for operation of the WCr and Syv towers was provided by the Department of Energy and the Ameriflux Network Management Project Support for UW CHEAS Cluster. Additional funding supporting WCr operations came from the Wisconsin Focus on Energy (EERD 10-06) and the USDA North Central Research Station. Additional support for Syv operations came from Department of Energy, Terrestrial Carbon Processes, now within the Terrestrial Ecosystem Science Program. We also thank Ahmed Tawfik and Travis O'Brien for helpful assistance with performing the model simulations and Frank Marsik for assistance with the calculation of advective moisture fluxes. Observational data are provided by the sources cited in this manuscript. NARR data are available at NOAA's Earth System Research Laboratory (<http://www.esrl.noaa.gov/psd/data/gridded/data.narr.html>). ERA data can be obtained from the ECMWF Data Server (<http://apps.ecmwf.int>). Users may obtain model output by contacting the corresponding author. Source code for RegCM is available at <https://gforge.ictp.it/gf/project/regcm/>.

- Changnon, S. A., and D. M. A. Jones (1972), Review of the influences of the Great Lakes on weather, *Water Resour. Res.*, *8*(2), 360–371.
- Collins, W. J., et al. (2011), Development and evaluation of an earth-system model—HadGEM2, *Geosci. Model Dev.*, *4*(4), 1051–1075.
- Cook, B. D., et al. (2004), Carbon exchange and venting anomalies in an upland deciduous forest in northern Wisconsin, USA, *Agric. For. Meteorol.*, *126*(3–4), 271–295.
- Croley, T. E. (1989), Verifiable evaporation modeling on the Laurentian Great Lakes, *Water Resour. Res.*, *25*(5), 781–792.
- Dai, A., F. Giorgi, and K. E. Trenberth (1999), Observed and model-simulated diurnal cycles of precipitation over the contiguous United States, *J. Geophys. Res.*, *104*(D6), 6377–6402.
- Dee, D. P., et al. (2011), The ERA-Interim reanalysis: Configuration and performance of the data assimilation system, *Q. J. R. Meteorol. Soc.*, *137*(656), 553–597.
- Derecki, J. A. (1981), Stability effects on Great Lakes evaporation, *J. Great Lakes Res.*, *7*(4), 357–362.
- Desai, A. R., P. V. Bolstad, B. D. Cook, K. J. Davis, and E. V. Carey (2005), Comparing net ecosystem exchange of carbon dioxide between an old-growth and mature forest in the upper Midwest, USA, *Agric. For. Meteorol.*, *128*(1–2), 33–55.
- Dunne, J. P., et al. (2012), GFDL's ESM2 global coupled climate-carbon Earth System Models. Part I: Physical formulation and baseline simulation characteristics, *J. Clim.*, *25*(19), 6646–6665.
- Dunne, J. P., et al. (2013), GFDL's ESM2 global coupled climate-carbon Earth System Models. Part II: Carbon system formulation and baseline simulation characteristics, *J. Clim.*, *26*(7), 2247–2267.
- Eltahir, E. A. B., and R. L. Bras (1994), Precipitation recycling in the Amazon basin, *Q. J. R. Meteorol. Soc.*, *120*(518), 861–880.
- Eltahir, E. A. B., and R. L. Bras (1996), Precipitation recycling, *Rev. Geophys.*, *34*(3), 367–378.
- Fritsch, J. M., and C. F. Chappell (1980), Numerical prediction of convectively driven mesoscale pressure systems. Part I: Convective parameterization, *J. Atmos. Sci.*, *37*(8), 1722–1733.
- Ghan, S. J., X. Bian, and L. Corsetti (1996), Simulation of the Great Plains low-level jet and associated clouds by general circulation models, *Mon. Weather Rev.*, *124*(7), 1388–1408.
- Giorgi, F., et al. (2012), RegCM4: Model description and preliminary tests over multiple CORDEX domains, *Clim. Res.*, *52*, 7–29.
- Goyette, S., N. A. McFarlane, and G. M. Flato (2000), Application of the Canadian regional climate model to the Laurentian Great Lakes region: Implementation of a lake model, *Atmos. Ocean*, *38*(3), 481–503.
- Grell, G. A. (1993), Prognostic evaluation of assumptions used by cumulus parameterizations, *Mon. Weather Rev.*, *121*(3), 764–787.
- Holman, K. D., A. Gronewold, M. Notaro, and A. Zarrin (2012), Improving historical precipitation estimates over the Lake Superior basin, *Geophys. Res. Lett.*, *39*, L03405, doi:10.1029/2011GL050468.
- Iorio, J. P., P. B. Duffy, B. Govindasamy, S. L. Thompson, M. Khairoutdinov, and D. Randall (2004), Effects of model resolution and subgrid-scale physics on the simulation of precipitation in the continental United States, *Clim. Dyn.*, *23*(3–4), 243–258.
- Jimenez, P. A., J. V.-G. de Arellano, J. Navarro, and J. F. Gonzalez-Rouco (2014), Understanding land-atmosphere interactions across a range of spatial and temporal scales, *Bull. Am. Meteorol. Soc.*, *95*(1), ES14–ES17.
- Legates, D. R., and C. J. Willmott (1990), Mean seasonal and spatial variability in gauge-corrected, global precipitation, *Int. J. Climatol.*, *10*(2), 111–127.
- Li, X., S. Zhong, X. Bian, W. E. Heilman, Y. Luo, and W. Dong (2010), Hydroclimate and variability in the Great Lakes region as derived from the North American Regional Reanalysis, *J. Geophys. Res.*, *115*, D12104, doi:10.1029/2009JD012756.
- Lofgren, B. M. (1997), Simulated effects of idealized Laurentian Great Lakes on regional and large-scale climate, *J. Clim.*, *10*(11), 2847–2858.
- Lofgren, B. M. (2004), A model for simulation of the climate and hydrology of the Great Lakes basin, *J. Geophys. Res.*, *109*, D18108, doi:10.1029/2004JD004602.
- Martin, G. M., et al. (2011), The HadGEM2 family of Met Office Unified Model climate configurations, *Geosci. Model Dev.*, *4*(3), 723–757.
- Mei, R., and G. Wang (2012), Summer land-atmosphere coupling strength in the United States: Comparison among observations, reanalysis data, and numerical models, *J. Hydrometeorol.*, *13*(3), 1010–1022.
- Mei, R., G. Wang, and H. Gu (2013), Summer land-atmosphere coupling strength over the United States: Results from the Regional Climate Model RegCM4-CLM3.5, *J. Hydrometeorol.*, *14*(3), 946–962.
- Mesinger, F., et al. (2006), North American regional reanalysis, *Bull. Am. Meteorol. Soc.*, *87*(3), 343–360.
- Mo, K. C., M. Chelliah, M. L. Carrera, R. W. Higgins, and W. Ebisuzaki (2005), Atmospheric moisture transport over the United States and Mexico as evaluated in the NCEP regional reanalysis, *J. Hydrometeorol.*, *6*(5), 710–728.
- Mu, Q., M. Zhao, and S. W. Running (2011), Improvements to a MODIS global terrestrial evapotranspiration algorithm, *Remote Sens. Environ.*, *115*(8), 1781–1800.
- Nave, L. E., et al. (2011), Disturbance and the resilience of coupled carbon and nitrogen cycling in a north temperate forest, *J. Geophys. Res.*, *116*, G04016, doi:10.1029/2011JG001758.
- New, M., M. Hulme, and P. Jones (2000), Representing twentieth-century space-time climate variability. Part II: Development of 1901–96 monthly grids of terrestrial surface climate, *J. Clim.*, *13*(13), 2217–2238.
- Notaro, M., K. Holman, A. Zarrin, E. Fluck, S. Vavrus, and V. Bennington (2013a), Influence of the Laurentian Great Lakes on regional climate, *J. Clim.*, *26*(3), 789–804.
- Notaro, M., A. Zarrin, S. Vavrus, and V. Bennington (2013b), Simulation of heavy lake-effect snowstorms across the Great Lakes basin by RegCM4: Synoptic climatology and variability, *Mon. Weather Rev.*, *141*(6), 1990–2014.
- Oleson, K. W., et al. (2004), Technical description of version 4.0 of the Community Land Model (CLM), *Tech. Rep. NCAR/TN-478+STR*, NCAR, Boulder, Colo.
- Oleson, K. W., et al. (2008), Improvements to the Community Land Model and their impact on the hydrological cycle, *J. Geophys. Res.*, *113*, G01021, doi:10.1029/2007JG000563.
- Pal, J. S., E. E. Small, and E. A. B. Eltahir (2000), Simulation of regional-scale water and energy budgets: Representation of subgrid cloud and precipitation processes within RegCM, *J. Geophys. Res.*, *105*(D24), 29,579–29,594.
- Petterssen, S., and P. A. Calabrese (1959), On some weather influences due to warming of the air by the Great Lakes in winter, *J. Meteorol.*, *16*(6), 646–652.
- Pressley, S., B. Lamb, H. Westberg, J. Flaherty, J. Chen, and C. Vogel (2005), Long-term isoprene flux measurements above a northern hardwood forest, *J. Geophys. Res.*, *110*, D07301, doi:10.1029/2004JD005523.
- Ruane, A. C. (2010), NARR's atmospheric water cycle components. Part I: 20-year mean and annual interactions, *J. Hydrometeorol.*, *11*(6), 1205–1219.
- Schär, C., D. Lüthi, U. Beyerle, and E. Heise (1999), The soil–precipitation feedback: A process study with a regional climate model, *J. Clim.*, *12*(3), 722–741.

- Schmid, H. P., H.-B. Su, C. S. Vogel, and P. S. Curtis (2003), Ecosystem-atmosphere exchange of carbon dioxide over a mixed hardwood forest in northern lower Michigan, *J. Geophys. Res.*, *108*(D14), 4417, doi:10.1029/2002JD003011.
- Scott, R. W., and F. A. Huff (1996), Impacts of the Great Lakes on regional climate conditions, *J. Great Lakes Res.*, *22*(4), 845–863.
- Seneviratne, S. I., T. Corti, E. L. Davin, M. Hirschi, E. B. Jaeger, I. Lehner, B. Orlowsky, and A. J. Teuling (2010), Investigating soil moisture-climate interactions in a changing climate: A review, *Earth Sci. Rev.*, *99*(3–4), 125–161.
- Sheffield, J., B. Livneh, and E. F. Wood (2012), Representation of terrestrial hydrology and large-scale drought of the continental United States from the North American Regional Reanalysis, *J. Hydrometeorol.*, *13*(3), 856–876.
- Sheffield, J., et al. (2013), North American climate in CMIP5 experiments. Part I: Evaluation of historical simulations of continental and regional climatology, *J. Clim.*, *26*(23), 9209–9245.
- Sousounis, P. J., and J. M. Fritsch (1994), Lake-aggregate mesoscale disturbances. Part II: A case study of the effects on regional and synoptic-scale weather systems, *Bull. Am. Meteorol. Soc.*, *75*(10), 1793–1811.
- Tawfik, A. B., and A. L. Steiner (2013), A proposed physical mechanism for ozone-meteorology correlations using land-atmosphere coupling regimes, *Atmos. Environ.*, *72*, 50–59.
- Trenberth, K. E. (1999), Atmospheric moisture recycling: Role of advection and local evaporation, *J. Clim.*, *12*(5), 1368–1381.
- Trenberth, K. E., and C. J. Guillemot (1998), Evaluation of the atmospheric moisture and hydrological cycle in the NCEP/NCAR reanalyses, *Clim. Dyn.*, *14*(3), 213–231.
- Turuncoglu, U. U., G. Giuliani, N. Elguindi, and F. Giorgi (2013), Modelling the Caspian Sea and its catchment area using a coupled regional atmosphere-ocean model (RegCM4-ROMS): Model design and preliminary results, *Geosci. Model Dev.*, *6*(2), 283–299.
- Vickers, D., M. Göckede, and B. E. Law (2010), Uncertainty estimates for 1-h averaged turbulence fluxes of carbon dioxide, latent heat and sensible heat, *Tellus B*, *62*(2), 87–99.
- Willmott, C. J., and K. Matsuura (2001), Terrestrial air temperature and precipitation: Monthly and annual time series (1950–1999). [Available at http://climate.geog.udel.edu/~climate/html_pages/Global2011/README.GlobalTSP2011.html.]
- Wright, D. M., D. J. Posselt, and A. L. Steiner (2013), Sensitivity of lake-effect snowfall to lake ice cover and temperature in the Great Lakes region, *Mon. Weather Rev.*, *141*(2), 670–689.
- Yao, S., Q. Huang, Y. Zhang, and X. Zhou (2013), The simulation of water vapor transport in East Asia using a regional air-sea coupled model, *J. Geophys. Res. Atmos.*, *118*, 1585–1600, doi:10.1002/jgrd.50089.
- Zangvil, A., D. H. Portis, and P. J. Lamb (2004), Investigation of the large-scale atmospheric moisture field over the midwestern United States in relation to summer precipitation. Part II: Recycling of local evapotranspiration and association with soil moisture and crop yields, *J. Clim.*, *17*(17), 3283–3301.
- Zeng, X., M. Shaikh, Y. Dai, R. E. Dickinson, and R. Myneni (2002), Coupling of the Common Land Model to the NCAR Community Climate Model, *J. Clim.*, *15*(14), 1832–1854.
- Zhong, S., X. Li, X. Bian, W. E. Heilman, L. R. Leung, and W. I. Gustafson Jr. (2012), Evaluation of regional climate simulations over the Great Lakes region driven by three global data sets, *J. Great Lakes Res.*, *38*(2), 212–225.